(Received 4 May 2024, Accepted 28 August 2024, Scheduled 4 September 2024)

Measurement of Time-Range-Angle-Dependent Beam Patterns of Frequency Diverse Arrays

Hao Chi Zhang[1, 5, *], Le Peng Zhang[1], Shengheng Liu[2], Zihuan Mao[2], Yahui Ma[3], Pei Hang He[1, 5], Wen Yi Cui[1], Yi Fei Huang[1, 5], Qi Yang[4, *], and Tie Jun Cui[1, 5, *]

[1] *State Key Laboratory of Millimeter Waves and Institute of Electromagnetic Space, Southeast University, Nanjing 210096, China*
[2] *School of Information Science and Engineering, Southeast University, Nanjing, China and with Purple Mountain Laboratories, Nanjing, China*
[3] *The China Academy of Electronics and Information Technology, Beijing 100041, China*
[4] *College of Electronic Science and Technology, National University of Defense Technology, Changsha 410073, China*
[5] *Zhangjiang Laboratory, Shanghai 201204, China*

ABSTRACT: Frequency diverse arrays (FDAs) have drawn great attention because they can provide a time-range-angle-dependent beam pattern that has many promising potential applications in navigation and radar systems. However, due to the limitations of measurement systems, this attractive beam pattern has not been experimentally observed. Here, a far-field measurement system for the time-range-angle beam pattern of FDA is proposed by improving the existing near-field mapping system. Without loss of generality, two types of time-range-angle-dependent beam patterns for FDA systems with different frequency sets are observed using the proposed far-field measurement system. The high efficiency and accuracy of the proposed system is verified by good agreement between the measured and simulated results. This work marks significant progress toward the practical implementation and application of FDAs.

1. INTRODUCTION

Phased array (PA) is one of the most versatile antennas, which can steer a beam by controlling the relative phases between elements. However, the switching interval of the beam state is restricted to milliseconds (ms) due to diode switching speed limitations, which limits the warning and searching radar applications that require fast scanning and response [1–3]. As an alternative to a PA, a frequency diverse array (FDA), in which the carrier frequency of each element is slightly distinguished, has been proposed to enable automatic beam scanning at a faster speed (the scanning period is not greater than nanoseconds) [4–6]. Owing to the degree of freedom in choosing the frequency for each element, an FDA can provide a range-angle-dependent beam pattern [4], which has drawn great attention in radio frequency stealth [5], low probability of interception radar [6], anti-interference systems [7], and secure wireless communication [8].

Since an FDA was first proposed by Antonik et al. in [4], many FDA schemes, including linear frequency-modulated continuous waveform [9], stepped frequency pulse [10, 11], and transmit subaperture schemes [12], have been proposed to construct radar with a fast automatically scanning beam. At present, most of the studies on FDAs have focused on the analysis of array characteristics and the design of the transmitting pattern [13–24]. Among them, some researchers have studied the range-dependent properties of transmitting beams and their applications in range fuzzy clutter suppression. The periodic scanning characteristics of the FDA beam have also been studied. In addition, researchers have carried out much research on FDA signal processing technology. However, traditional FDA schemes cannot be directly used in joint angle-range estimation due to their angle-range-coupled beam. To solve this problem, some particular frequency distributions, such as a nonlinear frequency offset [25, 26], a random frequency offset [27], and multicarrier distributions [28, 29], have been designed to achieve a range-angle-decoupled beam, which further enables joint angle-range estimation.

Although time-range-angle-dependent beam pattern is one of the most important features of an FDA, which exhibits a fundamental difference between PAs and FDAs [30], there is little research on experimental measurement of this unique beam pattern. An important reason is that the beam of an FDA not only is angle-distance dependent but also has fast time-varying characteristics (periods are often on the order of nanoseconds), which cannot be supported by the traditional far-field scanning system. In order to attempt to capture the fast time-varying electromagnetic field at different positions, some tries have been carried out. A double probe near-field scanner for measurement in the time domain is presented in [31, 32], which has proven to be useful in the measurement of frequency-hopping signals and the E-field on a printed circuit board (PCB). Although the above research has realized the measurement of time-varying E-fields, it is only applicable to near-field scanning. Ref. [33] carried out a study of time-varying EM far-field measurement of FDA system. However, this study only measured the angular-domain distribution of the time-varying EM-

* Corresponding authors: Hao Chi Zhang (hczhang0118@seu.edu.cn); Qi Yang (yangqi08@nudt.edu.cn); Tie Jun Cui (tjcui@seu.edu.cn).

field, which did not involve the distance domain at all. More importantly, the above researches use the rising or falling edge of the pulse signals captured at a fixed position as references to realize time-domain synchronization, which is not universal to all the measured systems. For example, the EM energy emitted by the common continuous wave FDA system does not have obvious rising or falling edge characteristics after synthesizing at a certain position. On the other hand, the above methods are greatly affected by the external environment, so when the Signal to Noise Ratio (SNR) of the reference signals captured in space decreases, the accuracy of time synchronization is difficult to be guaranteed. Therefore, considering the above two reasons, the measurement method with higher time-domain synchronization accuracy and stability is still to be explored.

In this article, we present an improved time synchronization technology to implement the far-field measurement of the time-range-angle-dependent beam pattern of an FDA system. Different from the existing time synchronization technology, the proposed method takes the standard periodic signal, e.g., sinusoidal signal, instead of pulse signal as the reference signal to achieve higher accuracy and stability of time synchronization. The experimental observation results are also in good agreement with numerical ones, which effectively verify the correctness of the theoretical model of FDA. In addition, some practical influencing factors, such as the inconsistency of radiation characteristics of the antenna unit in different directions and at different operating frequencies, the coupling effect between different channels, and spatial attenuation due to the air environment, are unavoidable and seriously affect the actual performance of an FDA system. These factors cannot be considered in theoretical models, but the proposed measurement method can obtain the theoretically ignored characteristics of an FDA, which would help optimize the system design.

The remaining sections of this article are organized as follows. Some theoretical properties of the FDA beam pattern related to experiments are firstly discussed in Section 2. Furthermore, an improved far-field time-domain measurement system and the detailed measurement method are introduced in Sections 3 and 4, respectively. The measured results of a common FDA (i.e., an FDA with a uniform frequency offset [UFO]) are reported in Section 5. In addition, the measured E-field and beam pattern of another FDA (i.e., an FDA with a nonuniform frequency offset [NUFO]) are further discussed. Conclusions are drawn in the final section.

2. FDA PROPERTIES

In this study, we consider a one-dimensional (1D) FDA made of N transmitting elements (TEs) with spacing d, as shown in Fig. 1(a). Different from a traditional PA, each TE generates EM radiation waves with different carrier frequencies. For the i-th element, the transmitted signal is given by

$$s_i(t) = \exp\left[j\left(2\pi f_i t + \varphi_i\right)\right] \tag{1}$$

where φ_i is the initial phase (i.e., the phase at the initial moment), and f_i is the radiation frequency of the i-th element, which can be further given by

$$f_i = f_0 + \Delta f_i \tag{2}$$

where f is the frequency of the first element, and Δf_i is the frequency offset of the i-th element. Without loss of generality, the total radiated signal $s_{total}(t)$ arriving at point (r, θ) in the far-field region can be expressed as (3),

$$\begin{aligned}
s_{\text{total}}(t) &= \frac{1}{r}\sum_{i=0}^{N-1} s_i\left(t-\tau_i\right) \\
&= \frac{1}{r}\sum_{i=0}^{N-1} \exp\left[j\left(2\pi f_i\left(t-\tau_i\right)+\varphi_i\right)\right] \\
&= \frac{1}{r}\sum_{i=0}^{N-1} \exp\left[j\left(2\pi\left(f_0+\Delta f_i\right)\left(t-\frac{r}{c}+\frac{id\sin\theta}{c}\right)+\varphi_i\right)\right] \\
&= \frac{\exp\left[j2\pi f_0\left(t-\frac{r}{c}\right)\right]}{r}\sum_{i=0}^{N-1} \exp\left[j\left(2\pi f_0\frac{id\sin\theta}{c}\right.\right. \\
&\left.\left.+2\pi\Delta f_i\left(\frac{id\sin\theta}{c}\right)+\varphi_i\right)+j2\pi\Delta f_i\left(t-\frac{r}{c}\right)\right]
\end{aligned} \tag{3}$$

In (3), $\tau_i = r/c - id\sin\theta/c$ is the delay time between the origin of the i-th element and the observation point. In addition, c is the speed of light. Note that the total radiated signal $s_{total}(t)$ can be measured. Furthermore, the pattern function (PF) $D(t, r, \theta)$ of the FDA can be calculated using (4),

$$\begin{aligned}
D(t,r,\theta) &= \sum_{i=0}^{N-1} \exp\left[j\left(2\pi f_0\frac{id\sin\theta}{c}+2\pi\Delta f_i\left(\frac{id\sin\theta}{c}\right)\right.\right. \\
&\left.\left.+\varphi_i\right)+j2\pi\Delta f_i\left(t-\frac{r}{c}\right)\right] \\
&= e^{j\varphi_0}+\sum_{i=1}^{N-1} \exp\left[j2\pi f_0\frac{id\sin\theta}{c}+j\varphi_i+j2\pi\Delta f_i\left(\frac{id\sin\theta}{c}\right)\right. \\
&\left.+j2\pi\Delta f_i\left(t-\frac{r}{c}\right)\right] \\
&= e^{j\varphi_0}+\sum_{i=1}^{N-1} D_{1i}(\theta)D_{2i}(\theta)D_{3i}(t,r)
\end{aligned} \tag{4}$$

From (4), we clearly observe that each term of PF D of the FDA can be rewritten as the product of three parts (i.e., $D_{1i}(\theta)$, $D_{2i}(\theta)$, and $D_{3i}(tr)$) with different characters. The first term $D_{1i}(\theta)$ is exactly consistent with that of a conventional PA. The second term $D_{2i}(\theta)$ is an angle-dependent item unique to FDA systems which affects the initial radiation direction of the array. The last term $D_{3i}(tr)$ is the time-range-dependent item leading to a shaped beam pattern, which is regarded as one of the most prominent features of an FDA. Here, to simplify the analysis, the effects of mutual coupling and the beam pattern of the elements are ignored in this qualitative analysis process. Notably, both mutual coupling and the element beam pattern are range- and time-independent, which does not lead to a range-time-dependent beam pattern. In other words, the range-time-dependent beam pattern is an intrinsic FDA attribute.

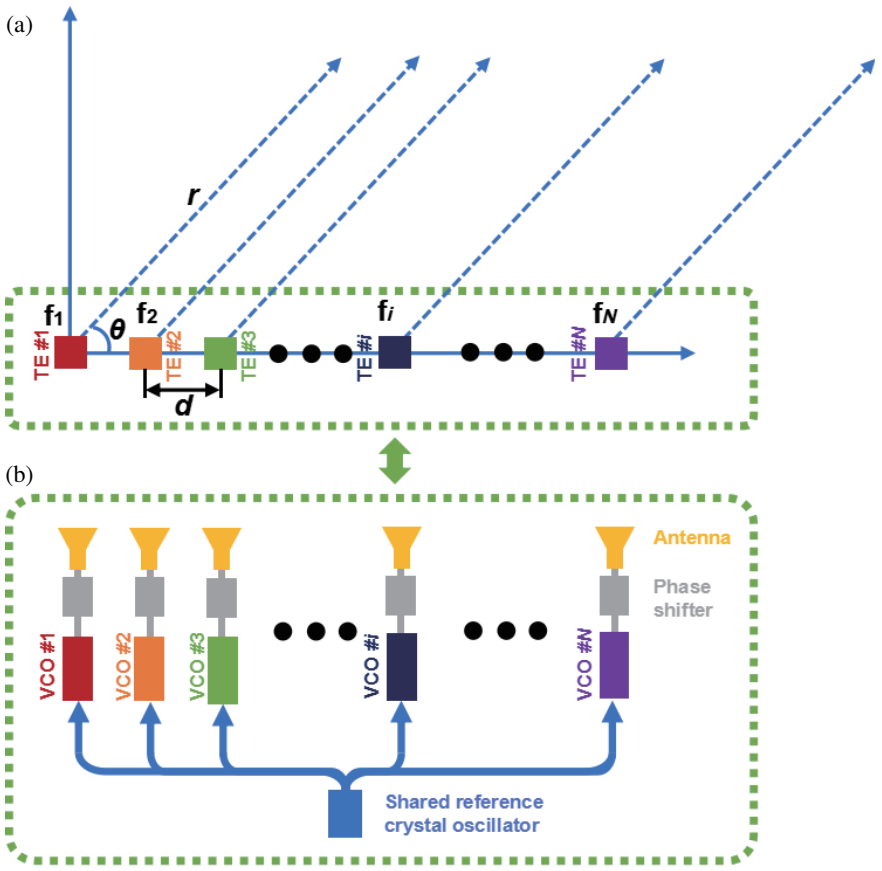

FIGURE 1. (a) Configuration of the FDA. This FDA is made of N TEs with spacing d, in which the first TE is regarded as the reference TE and its position is chosen as the origin of the coordinates. (b) Schematic diagram of the generic FDA prototype system, which is composed of a 100 MHz-shared reference crystal oscillator and N wide-angle antennas, N phase shifters, and N voltage-controlled oscillators.

Before discussing the detailed measurement method, here, we further investigate the time-dependent properties of the PF $D(t,r,\theta)$ of an FDA system. According to (4), it depends on the time-dependent properties of $D_{3i}(tr)$. However, demonstrating the existence of a time-domain period for all FDA systems is impossible. Nevertheless, for actual FDA systems, the transmitted frequency produced by the local oscillator (LO) can be only selected as an integral multiple of the minimum scale Δf_{LO} (i.e., the minimum LO step). Hence, the frequency offset of the i-th element Δf_i can be further expressed as $m_i \Delta f_{LO}$ ($i = 1, 2, 3 \ldots$), in which m_i is the corresponding integer of the i-th frequency offset. In this case, $D_{3i}(tr)$ can be further given as:

$$D_{3i}\left(t+\frac{1}{\Delta f_{LO}},r\right)=\exp\left[j2\pi m_i\Delta f_{LO}\left(t+\frac{1}{\Delta f_{LO}}-\frac{r}{c}\right)\right]$$

$$=\exp\left[j2\pi m_i\Delta f_{LO}\left(t-\frac{r}{c}\right)+j2\pi m_i\right]=D_{3i}\left(t,r\right) \quad (5)$$

This shows that all $D_{3i}(tr)$ ($i = 1, 2, 3 \ldots$) have the same period $1/\Delta f_{LO}$. Hence, PF $D(t,r,\theta)$ is a periodic function, which implies periodic beam behavior of the FDA. In fact, for an actual FDA system, the real period can be easily obtained as $1/m\Delta f_{LO}$, where m is the greatest common divisor of m_1, m_2, …, m_{N-1}. However, note that the frequency of the first element f is also an integral multiple of the minimum scale Δf_{LO}, recorded as $f = q\Delta f_{LO}$. Hence, the total radiated signal $s_{total}(t)$ is also periodic, whose period can be determined by $1/q_1\Delta f_{LO}$, where q_1 is any common divisor of m and $q0$. It is the unique periodic beam behavior of FDA that provides an effective approach to realize time synchronization by using the signal generated by the crystal oscillator of FDA transmitter as reference.

To show the beam patterns of FDAs with different frequencies, we use a homemade FDA prototype system based on spoof surface plasmon polariton technology [34], which is composed of a series of transmitting links (TLs) with different frequencies and a 100 MHz shared reference crystal oscillator connected to each TL using an N-way power divider, as shown in Fig. 1(b). In this design, the i-th TL is composed of a wide-angle antenna, a phase shifter, and a voltage-controlled oscillator (VCO) with frequency f_i. In this system, the phase shifter and shared reference crystal oscillator are used to maintain all links with the same frequency primarily standard. To facilitate a comparison of the measured and calculated results, we make all initial TE phases consistent by carefully adjusting the phase shifter.

One of the most important advantages of the proposed system is that it can easily switch between different frequency offsets based on a single system. This can help us control other irrelevant variables, for example, the machining error between dif-

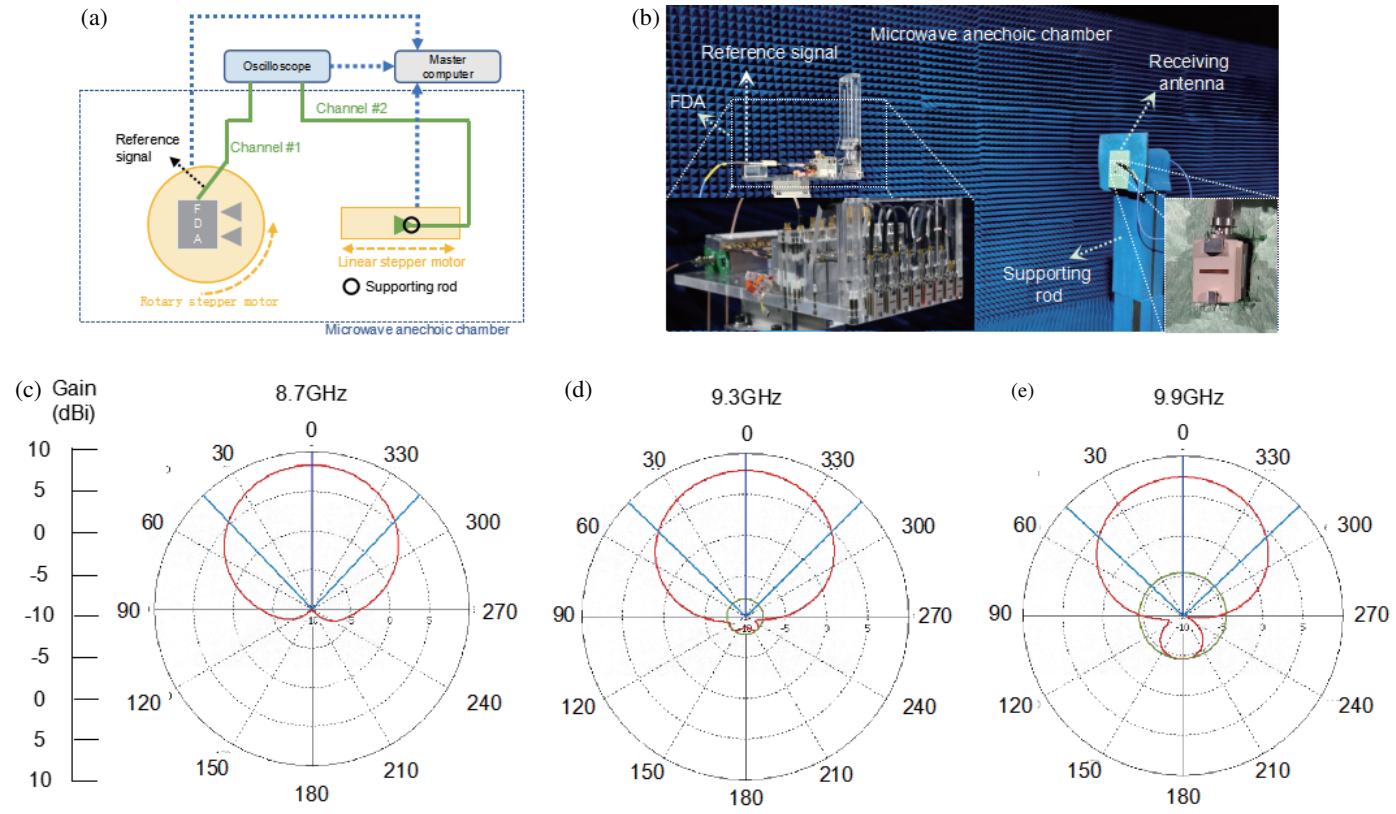

FIGURE 2. (a) Configuration of the measurement system, which is an upgraded traditional far-field measurement system. This system is composed of a measured FDA transmitted system, a rotary stepper motor with a stage, a linear stepper motor, a supporting rod, a receiving antenna, an oscilloscope with two synchronous sampling channels, and a master computer used to control the motors and oscilloscope. Noted that the center of the FDA transmitter antenna array is located at the rotating center of the rotary motor (b) Photographs of the measurement system, FDA and receiving antenna. A detailed view of the FDA transmitted system and receiving antenna is shown in the inset. (c) Radiation patterns of the antennas unit at 8.7 GHz. (d) Radiation patterns of the antennas unit at 9.3 GHz. (e) Radiation patterns of the antennas unit at 9.9 GHz.Without loss of generality, we use the planar half-wave dipole antenna as the transmitting and receiving antenna unit, where the transmitting antenna is a 8-element linear array of and the receiving antenna consists of only one unit. Each unit has the same size (11.62 mm $*$ 11.62 mm). The operating bandwidth of the antenna unit covers 8.7–9.9 GHz and its half-power beam-width is greater than $\pm 45^{\circ}$.

ferent samples. Without loss of generality, two common kinds of FDAs are implemented for real measurements using this prototype system. One is an FDA with a linear gradient frequency offset (LGFO) (i.e., $\Delta f_i = i\Delta f_1$), and the other is an FDA with a nonlinear gradient frequency offset (NLGFO). We select two common frequency sets in the X band for the experiment, as shown in Table 1.

3. FAR-FIELD TIME-DOMAIN MEASUREMENT SYSTEM

In this section, we discuss the details of the measurement system. Considering the time range-dependent properties of the FDA beam pattern, the proposed measurement system should have the ability to sample at different times, ranges, and angles. However, traditional far-field measurement systems only have rotating motors, which makes the systems have only angle scanning [33]. In other words, we need to improve the traditional systems so that time and distance scanning can be achieved. On the one hand, to achieve range scanning, we install a far-field receiving horn on a controlled linear stepper motor rather than directly at the far end of the microwave anechoic chamber, as shown in Fig. 2(a). With the help of this linear stepper motor, the far-field receiving horn can move in the radial direction, which makes the measurement system capable of range scanning. We also cover the surface of the stepper motor structure and other support structures with absorbing materials to avoid the influence of EM wave radiation. On the other hand, adding time scanning to the system requires obtaining far-field information at different points at the same time over a certain period, which is almost impossible for an actual measurement system. To solve this problem, we propose a periodic extension method based on the periodic properties of the FDA beam pattern. Because this method can use the signal measured in any period for periodic extension, it allows the measurement of far-field signals at different positions and at different times, which can be implemented through mechanical scanning. However, to ensure time synchronization in the whole measurement, we propose to synchronously sample a periodic signal (e.g., a periodic sine wave signal) as a reference signal. More importantly, considering the signal coherence, we suggest using the signal related to the output of the shared reference crystal oscillator

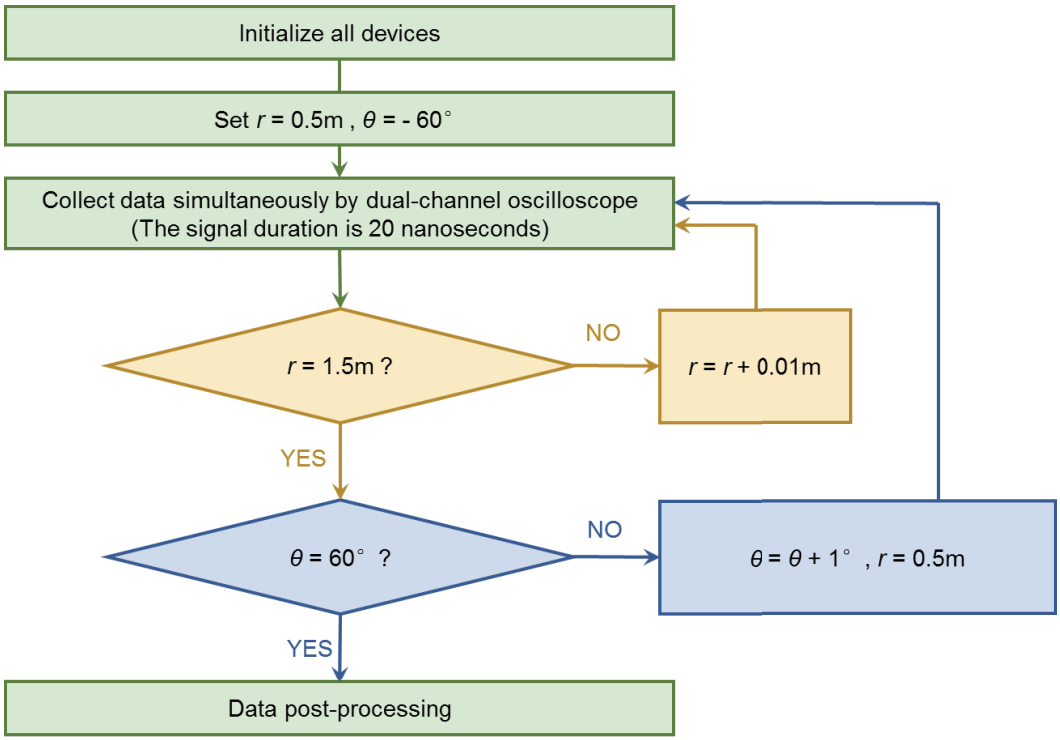

FIGURE 3. Schematic diagram of the measurement process.

TABLE 1. FDA system frequency sets.

TE Label	LGFO Scheme		NLGFO Scheme	
	Frequency	Frequency Offset	Frequency	Frequency Offset
0	9.00 GHz	0.00 GHz	9.00 GHz	0.00 GHz
1	9.10 GHz	0.10 GHz	9.17 GHz	0.17 GHz
2	9.20 GHz	0.20 GHz	9.30 GHz	0.30 GHz
3	9.30 GHz	0.30 GHz	9.35 GHz	0.35 GHz
4	9.40 GHz	0.40 GHz	9.53 GHz	0.53 GHz
5	9.50 GHz	0.50 GHz	9.58 GHz	0.58 GHz
6	9.60 GHz	0.60 GHz	9.64 GHz	0.64 GHz
7	9.70 GHz	0.70 GHz	9.70 GHz	0.70 GHz

as the reference signal, and its period is $1/q_1\Delta f_{LO}$. According to this idea, far-field information and reference signals must be synchronously sampled over a period using an oscilloscope. In our measurement, the output of the 100 MHz shared reference crystal oscillator and its decade frequency division are selected as the reference signals of the FDAs using the LGFO and NLGFO schemes, respectively.

According to the above ideas, we upgrade a traditional far-field measurement system to meet the requirements for FDA measurements. This customized far-field measurement system is composed of three modules: a transmitter, a receiver, and a data collector, as shown in Fig. 2(a). First, the transmitter module includes the measured FDA system, a high-accuracy rotary stepper motor, and a stage. In our measurement, the FDA transmitter is installed on the stage, which is fixed on the rotary stepper motor controlled by a master computer, whose accuracy and minimum angle step size are 0.03° and 0.1°, respectively. Through such designs, we can sweep the observed angle with an interval of 1° in the region of interest. The center of the FDA transmitter antenna array is deliberately placed in the rotating center of the rotatory motor. Second, the receiver module is composed of a receiver antenna, a supporting rod, and a high-accuracy linear stepper motor. In the measurement, the receiver antenna is fixed on the supporting rod, and the linear stepper motor is used to carry the whole receiving part in the radial direction, whose accuracy and minimum step are 0.05 mm and 0.1 mm, respectively. This design makes sweeping in the radial direction possible with an interval of 10 mm. Between

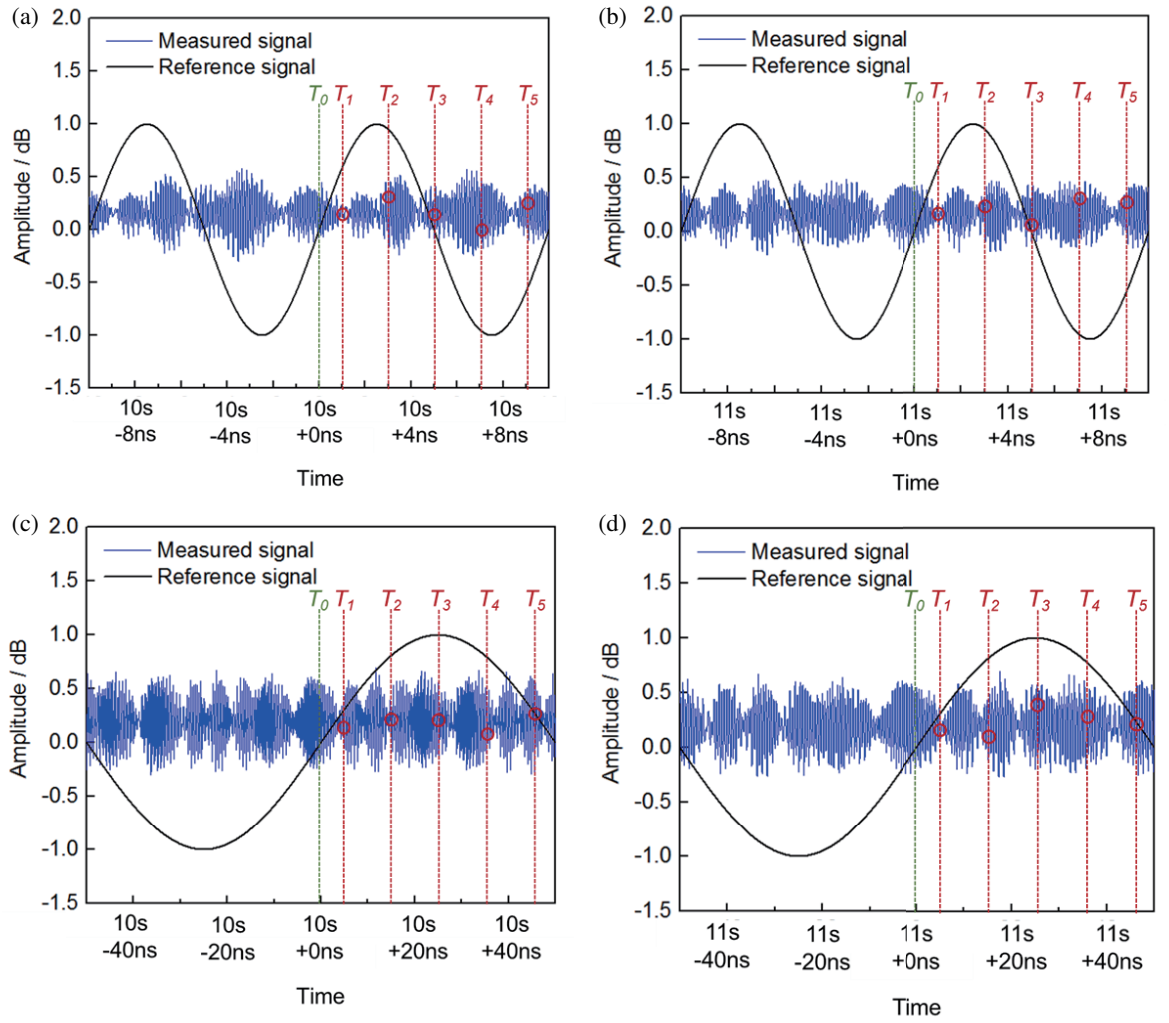

FIGURE 4. (a) Results of the measured signal and reference signal (sinusoidal) of the FDA system using the LGFO scheme sampled at $(-30°, 1.00\,\text{m})$. (b) Results of the measured signal and reference signal (sinusoidal) of the FDA system using the LGFO scheme sampled at $(-30°, 1.01\,\text{m})$. (c) Results of the measured signal and reference signal (sinusoidal) of the FDA system using the NLGFO scheme sampled at $(-30°, 1.00\,\text{m})$. (d) Results of the measured signal and reference signal (sinusoidal) of the FDA system using the NLGFO scheme sampled at $(-30°, 1.01\,\text{m})$.

the transmitter and receiver, a clock signal is linked through the coaxial line cable to ensure the synchronization. Since the cable delay is the same at different collection points, the field distribution measurement can still be equivalent to simultaneous. In other words, the received signal of all collection points is equivalent to a same translation in the time domain. Third, the data collector module is composed of a digital storage oscilloscope (Agilent DSO91304A) with two synchronous sampling channels and a master computer that simultaneously controls the motors and oscilloscope to automate the sampling process at different spatial positions.

4. FDA TIME-RANGE-ANGLE-DEPENDENT BEAM PATTERN MEASUREMENT METHOD

Based on the above measurement system, we propose a measurement method for the FDA time-range-angle-dependent beam pattern. The measurement process is shown in Fig. 3. Before testing, we should fix the FDA transmitter on the stage with a rotary stepper motor and fix the receiver on the supporting rod with a linear stepper motor. To minimize the impact of the environment, we can cover the surface of the stepper motor and other support structures with absorbing materials. In this measurement example, the initial position of the distance domain is set to 0.5 m, and the initial position of the angle domain is set to $-60°$. Next, the data are collected simultaneously by dual-channel oscilloscope, and the signal duration is set to 20 nanoseconds. Then, the distance-domain motor drives the receiving horn to move to the next position in a preset step (0.01 m) until the distance-domain position reaches 1.5 m. In our opinion, there are two main factors that determine the sampling distance range. On the one hand, the radial distance must satisfy the far field condition of the antenna array. By calculation, the far field condition of the antenna used is greater than 0.57 m. On the other hand, too far radial distance will lead to weak electromagnetic field energy, which is not conducive to the accuracy and reliability of the measurement. Taking the above reasons into consideration, we

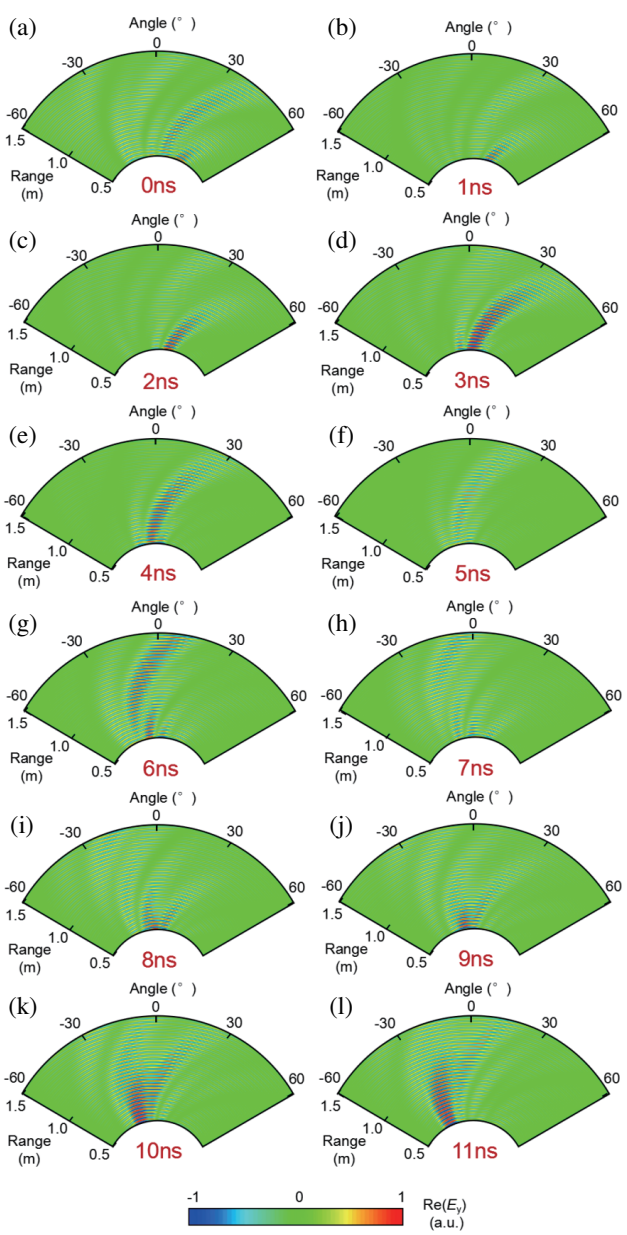

FIGURE 5. Simulated E-field distribution of the FDA system using the LGFO scheme. (a) 0 ns; (b) 1 ns; (c) 2 ns; (d) 3 ns; (e) 4 ns; (f) 5 ns; (g) 6 ns; (h) 7 ns; (i) 8 ns; (j) 9 ns; (k) 10 ns; (l) 11 ns.

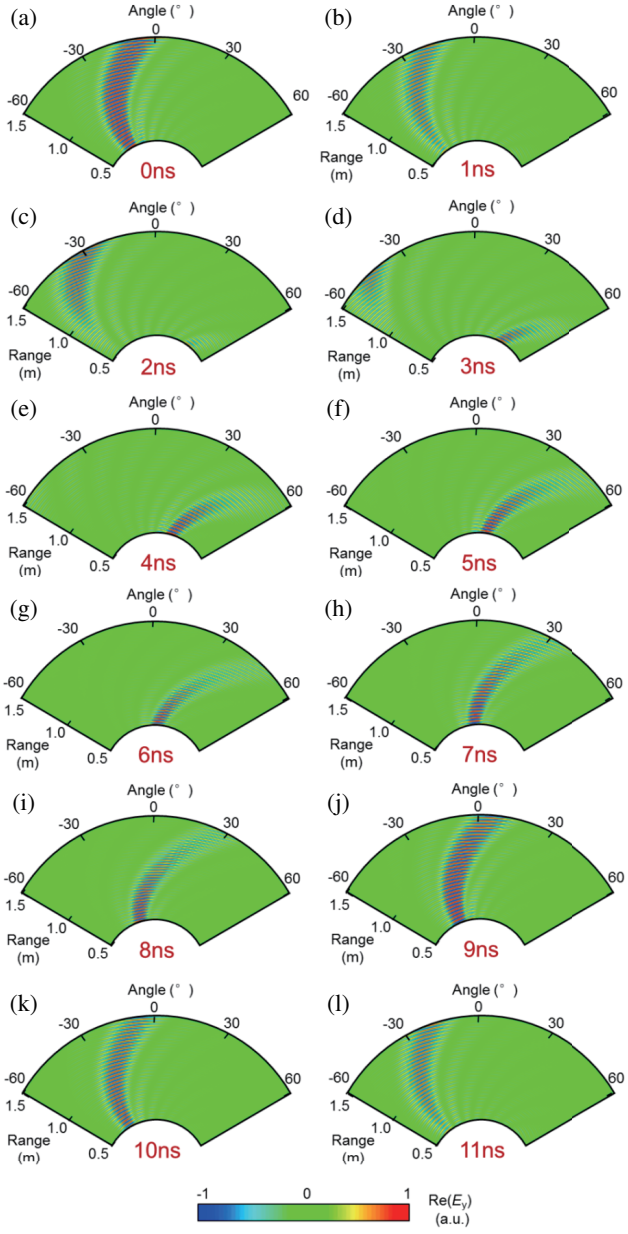

FIGURE 6. Measured E-field distribution of the FDA system using the LGFO scheme. (a) 0 ns; (b) 1 ns; (c) 2 ns; (d) 3 ns; (e) 4 ns; (f) 5 ns; (g) 6 ns; (h) 7 ns; (i) 8 ns; (j) 9 ns; (k) 10 ns; (l) 11 ns.

determined the radial distance range to be 0.5 to 1.5 m. In a similar way, the angle-domain motor turns the FDA transmitter in a preset step (1°) until the angle-domain position reaches 60°. When the space traversals in range and angle domain are both completed, the data measured at different positions are all stored and processed. Finally, the spatial distribution of the E-field or beam pattern can be plotted. Note that the amplitude-phase calibration of different FDA elements is not mentioned in the measurement process. The calibration of amplitude and phase is intended to improve FDA system performance and is not part of the study of the measurement. In other words, even without calibration, the proposed method should be able to observe the corresponding field distribution.

Different from traditional far-field measurement methods, the proposed method has the capability to measure the time-varying field distribution of FDA systems with continuous-wave scheme, which is realized by introducing the time reference signal. Notably, the period of the reference signal must be equal to the FDA beam-scanning period (in this measurement example, period is 10 ns). Since the principles are the same, we take the measurement of the LGFO scheme as an example. Without loss of generality, we assume that we want to measure the E-field distribution at time T_1, and the time corresponding to the zero value of the rising edge of the reference signal is defined as time T. According to the above process, the position of the receiving antenna is constantly adjusted, and the signals

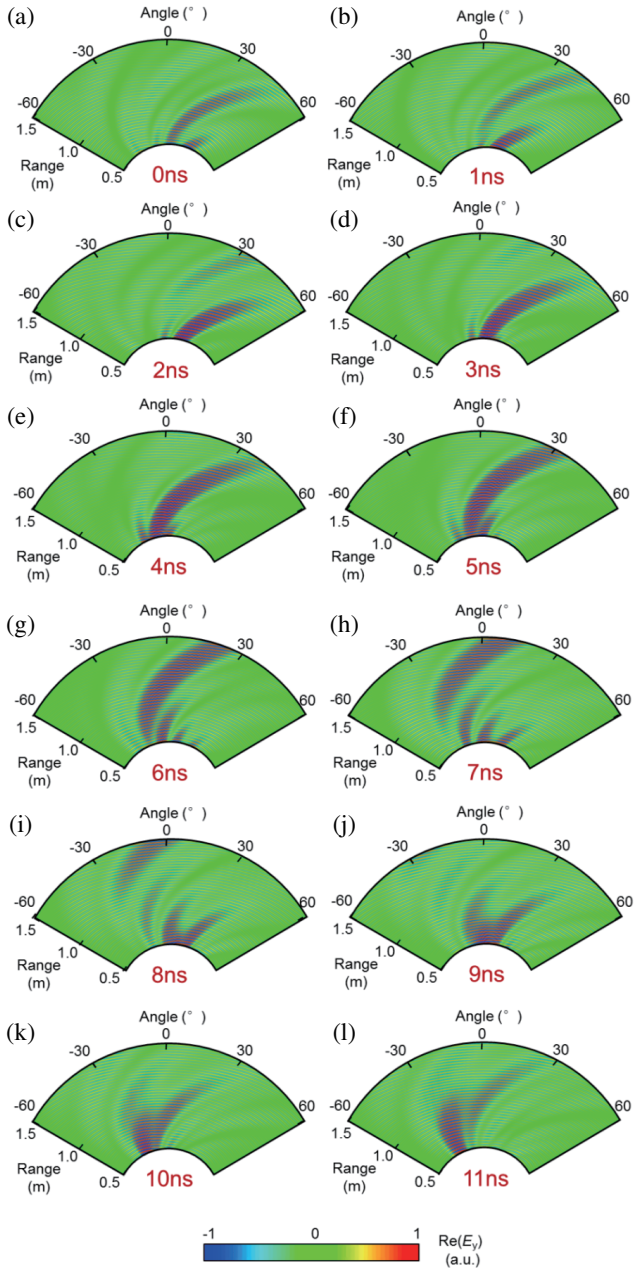

FIGURE 7. Simulated E-field distribution of the FDA system using the NLGFO scheme. (a) 0 ns; (b) 1 ns; (c) 2 ns; (d) 3 ns; (e) 4 ns; (f) 5 ns; (g) 6 ns; (h) 7 ns; (i) 8 ns; (j) 9 ns; (k) 10 ns; (l) 11 ns.

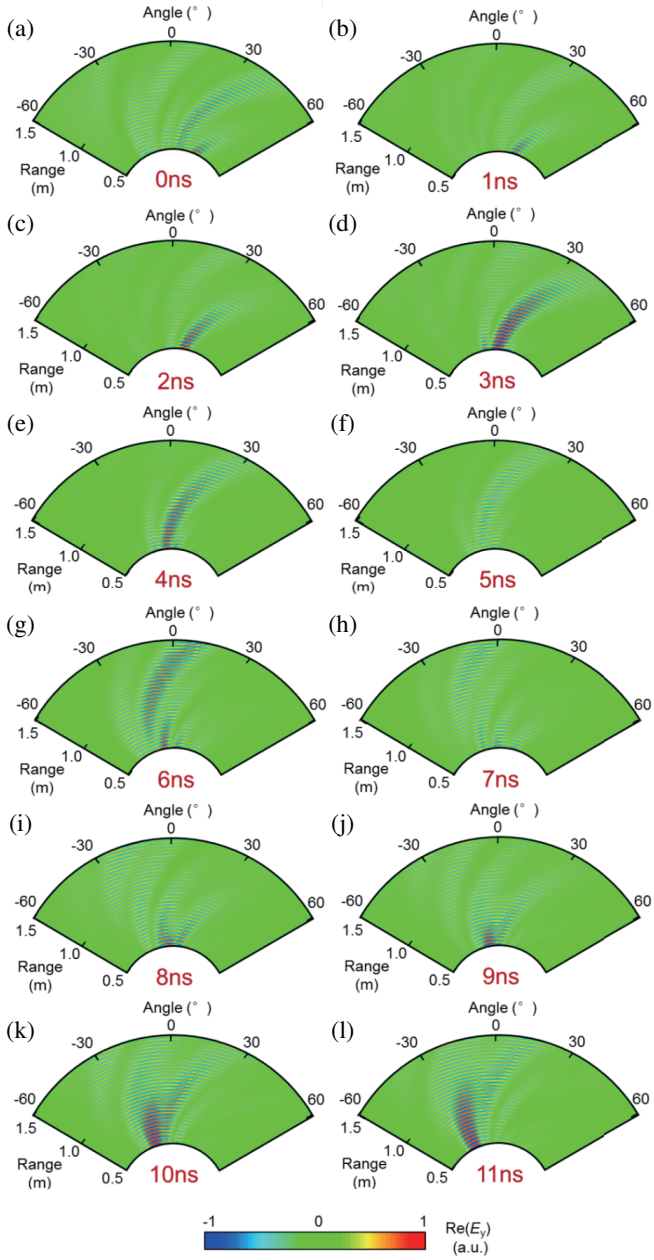

FIGURE 8. Measured E-field distribution of the FDA system using the NLGFO scheme. (a) 0 ns; (b) 1 ns; (c) 2 ns; (d) 3 ns; (e) 4 ns; (f) 5 ns; (g) 6 ns; (h) 7 ns; (i) 8 ns; (j) 9 ns; (k) 10 ns; (l) 11 ns.

at different positions are recorded for more than one period until the whole area is traversed. In Figs. 4(a) and 4(b), we randomly display the measured signal sampled at $(-30°, 1.00\,\text{m})$ and $(-30°, 1.01\,\text{m})$. Although the sampling process at these two positions is carried out in turn, the field distributions can be considered to be equivalent to those obtained with simultaneous acquisition if the time difference from time T is $(T_1 - T)$. Similarly, the measured results at all positions are equivalent to those obtained simultaneously using this method. Since we set the interval for the receiving antenna to move to the next sampling position at 1 second, time T difference in Figs. 4(a) and 4(b) is exactly 1 second. In addition, Figs. 4(c) and (d) show the measured signals obtained in the measurement of the FDA system using the NLGFO scheme. Because the time-varying period of the field distribution is different, the selected reference signal period is also different. In addition, it can be clearly seen from Fig. 4 that the SNR of periodic signals captured in space decreases without obvious rising or falling edge characteristics, which seriously deteriorates the accuracy of time synchronization in [31–33]. Besides, although the vibration of the motor is inevitable, the data is collected in the static state after the probe movement is completed. So, the effect of motor vibration on data acquisition can be negligible.

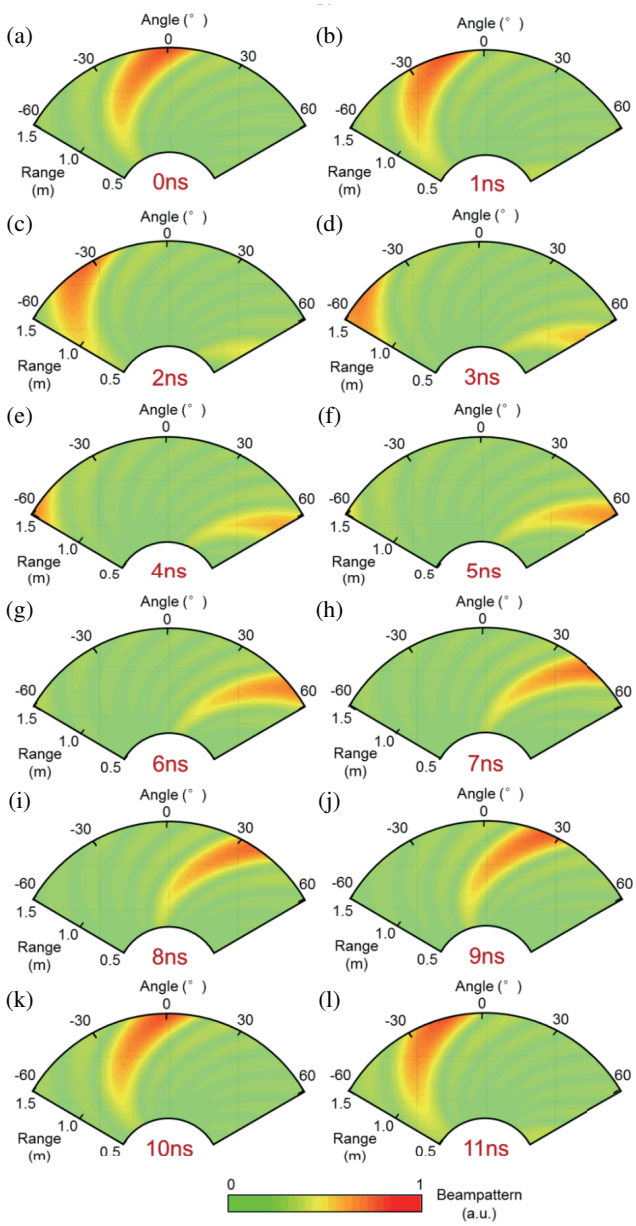

FIGURE 9. Calculated beampattern of the FDA system using the LGFO scheme. (a) 0 ns; (b) 1 ns; (c) 2 ns; (d) 3 ns; (e) 4 ns; (f) 5 ns; (g) 6 ns; (h) 7 ns; (i) 8 ns; (j) 9 ns; (k) 10 ns; (l) 11 ns.

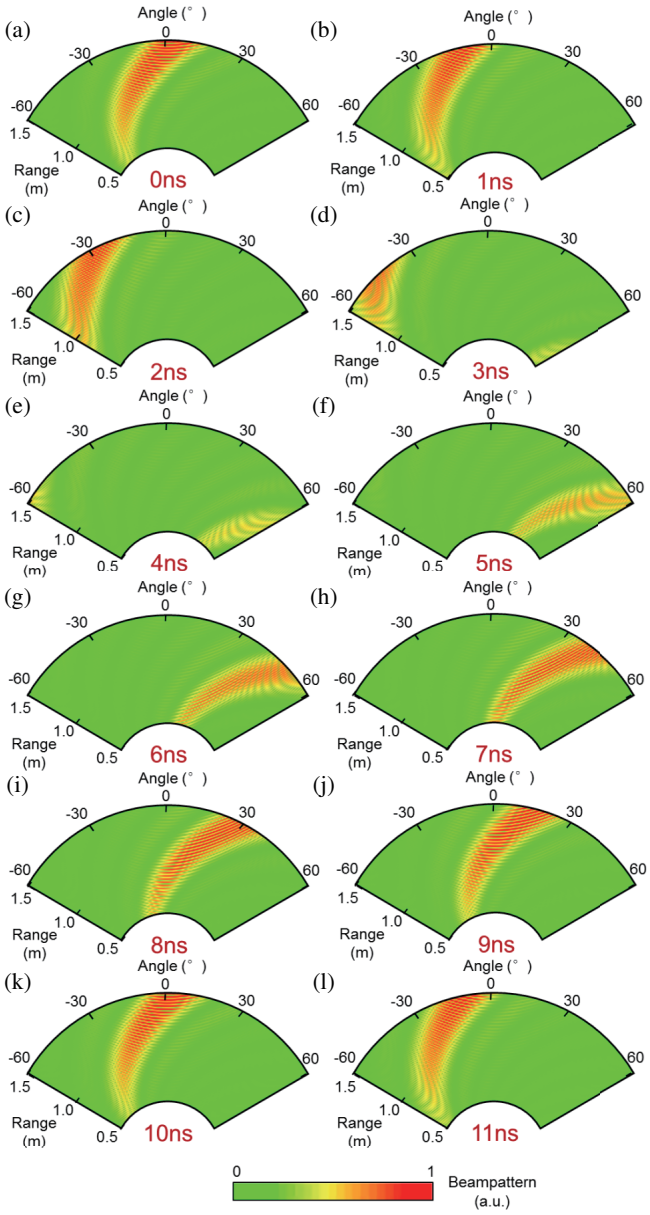

FIGURE 10. Measured beampattern of the FDA system using the LGFO scheme. (a) 0 ns; (b) 1 ns; (c) 2 ns; (d) 3 ns; (e) 4 ns; (f) 5 ns; (g) 6 ns; (h) 7 ns; (i) 8 ns; (j) 9 ns; (k) 10 ns; (l) 11 ns.

5. ANALYSIS OF THE MEASURED RESULTS

To verify the validity of the proposed method, we measure the E-field distribution of the FDA system using the LGFO and NLGFO schemes, and the measurement results are compared with the simulated ones. It is worth mentioning that commercial simulation software "CST Microwave Studio" is used to complete all simulation. The simulated E-field distribution of the FDA system using the LGFO scheme is shown in Fig. 5. Without loss of generality, we select the results at $t = 0$, 1, 2, 3, 4, 5, 6, 7, 8, 9, 10, and 11 ns as representative examples to show the time-varying characteristics of the E-field distribution. As predicted, the E-field distribution of this FDA system presents a curve shape, and the time-varying period is exactly 10 ns ($1/\Delta f$). As shown in Fig. 6, both the measured curve-shaped distribution and time-varying period are in good agreement with the simulated results, which confirms the effectiveness of the proposed method. In our opinion, there are two main factors in the determination of the sampling density. On the one hand, the number of acquisition points should be enough to ensure that the observed field distribution performance can be fully revealed. On the other hand, sampling density is also limited by time cost, and too many sampling points would lead to unnecessary time cost. According to the empirical principle, 0.4 to 0.6 wavelength is usually selected as the collection point spacing (The angular interval can be determined by the radial distance of the center). Taking the above two factors into con-

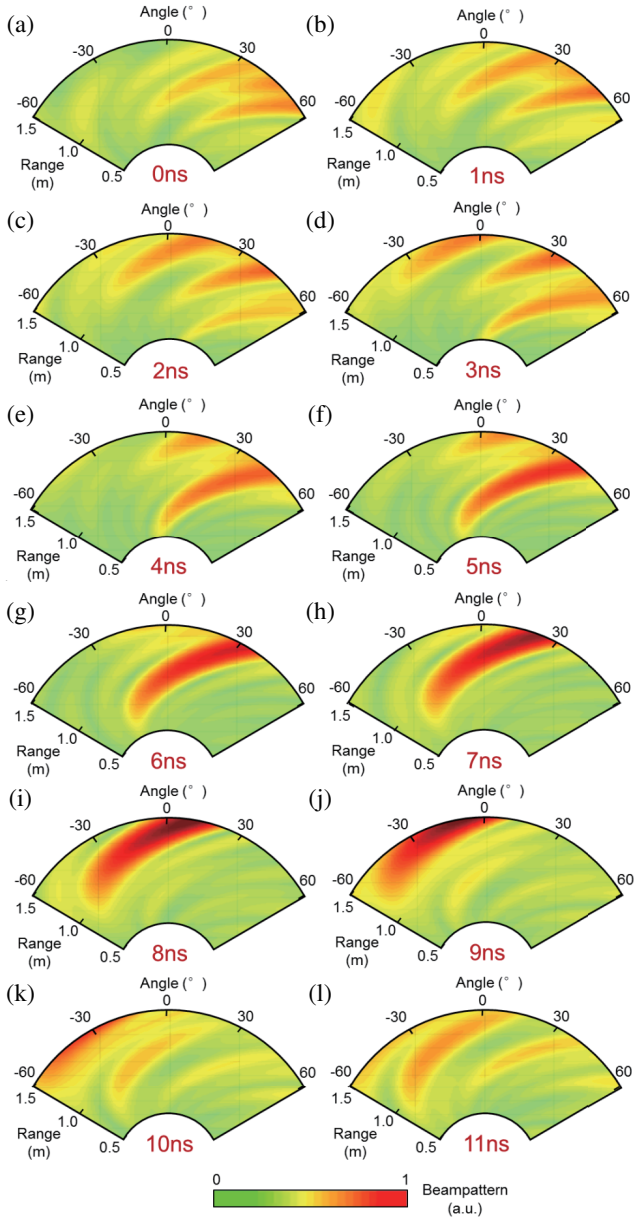

FIGURE 11. Calculated beampattern of the FDA system using the NLGFO scheme. (a) 0 ns; (b) 1 ns; (c) 2 ns; (d) 3 ns; (e) 4 ns; (f) 5 ns; (g) 6 ns; (h) 7 ns; (i) 8 ns; (j) 9 ns; (k) 10 ns; (l) 11 ns.

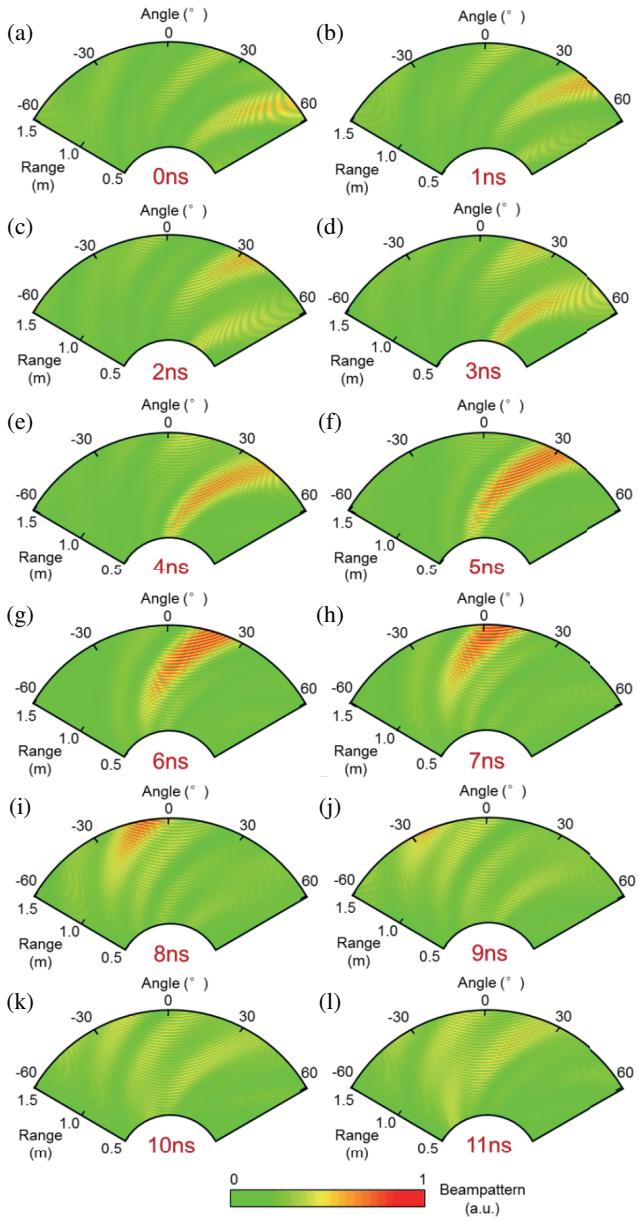

FIGURE 12. Measured beampattern of the FDA system using the NLGFO scheme. (a) 0 ns; (b) 1 ns; (c) 2 ns; (d) 3 ns; (e) 4 ns; (f) 5 ns; (g) 6 ns; (h) 7 ns; (i) 8 ns; (j) 9 ns; (k) 10 ns; (l) 11 ns.

sideration, we choose a range-step of 10 mm and an angle-step of 1 degree. The final sample number is approximately 12,221. Depending on the speed of rotation or movement of the motor, each sampling time is 1 second. Therefore, the total time for a typical measurement process, for example, that shown in Fig. 6, is approximately three hours and forty minutes. Similarly, the simulated and measured results of the FDA system using the NLGFO scheme are shown in Figs. 7 and 8. Although the E-field distribution of the NLGFO scheme is more chaotic than the LGFO scheme, the measured and simulated results also show good agreement.

Although the measured results are consistent with the simulated ones, there remain several differences. (1) Compared to the simulated results, narrower beams are shown in the measured results. This may be because real antennas can hardly achieve the same directivity as simulated antennas. Additionally, the amplitude fluctuation of different frequency signals is not considered in the simulation. (2) The measured values of the E-field are slightly smaller than the simulated results, which may result from the inevitable attenuation due to transmission loss and port reflection. In other words, the measured results show a more practical E-field distribution of the FDA system, which cannot be realized by means of theoretical and simulation studies.

In addition to the measurement of the E-field, we also obtain the measured beam pattern based on formula (4). Notably,

the data we sampled at every position are the real values of the E-field, but the complex values of the measured signals can be multiplied using the Hilbert transform, which can be further used to obtain the beam pattern. Using the commercial software MATLAB, the beam pattern of the FDA using the LGFO scheme can be calculated, as shown in Fig. 9, and the measured results are shown in Fig. 10. Clearly, the measured results are in good agreement with the calculated ones, which proves that the proposed method is also capable of measuring time-varying beam patterns. Beam pattern measurement of the FDA system using the NLGFO scheme is also carried out. The calculated and measured results are shown in Figs. 11 and 12, which also show good consistency.

Note that the above experimental observations are only represented by a few examples, and the method has certain universality in the aspects of signal waveform, number of elements, etc. For example, as long as the spatial EM field distribution has periodic time-varying characteristics and the reference signal is selected appropriately, the proposed method can be applied to any kinds of waveform such as continuous wave and pulse wave. Similarly, the method can be applied to arrays of any size in principle, and the above experiments only take the eight-channel transmitter as examples.

Although the measured beam patterns are in good agreement with the simulated results, there are still some differences, and the possible causes of the error are summarized as follows. (i) In practice, there is inherent coupling between adjacent transmitting antennas, which is not accounted for in the theoretical model, and there are unavoidable errors in the frequency accuracy and initial phases of the actual transmitted signals. As widely acknowledged, the inevitable phase noise of the RF source will lead to the error of the frequency and the initial phase, and this error is random. Therefore, given this randomness, the above errors are difficult to fully evaluate in simulations. (ii) Due to the pattern characteristics of the antennas, there are errors in the actual measurement of different angles, especially in the case of large angles. (iii) The impact of environmental and instrument noise is also unavoidable. (iv) Limited by the sampling rate of the oscilloscope, there is a quantization error when the measured signals are sampled. In this measurement, the Agilent Infiniium DSO91304A oscilloscope is used to collect the received signals with a bandwidth of 13 GHz and a maximum sampling rate of 40 GSa/s. The introduction of advanced digital signal processing technology is expected to improve the measurement method and further improve the measurement accuracy.

6. CONCLUSION

In this paper, an improved measurement system to observe the beam pattern of an FDA by introducing an extra time reference signal and a stepper motor in the radial direction is proposed. We discuss some important properties of the FDA beam pattern. An improved far-field time-domain measurement system and a detailed measurement method are introduced. To verify the validity of the proposed method, we carry out measurements of the E-field distribution and beam pattern of an FDA system using the LGFO and NLGFO schemes, and the measurement results are compared with the simulated/calculated ones, which show good consistency. In addition, we further analyze the causes of the differences between the measured and simulated results, such as the amplitude fluctuation in the angle domain and frequency domain and the coupling effect between different channels. By means of the proposed method, some field distribution characteristics, which are different from those for the theoretical model, are observed. The measured results show more realistic characteristics of FDA systems, which will help improve the design and performance of FDA systems. The proposed method not only helps us study FDA systems from a more realistic perspective but also has significance for other space-time coding systems.

DECLARATION OF COMPETING INTEREST

The authors declare that they have no conflict of interest.

ACKNOWLEDGEMENT

This work was supported by the National Defense Basic Research Projects under Grant No. JCKY2022203C039, National Natural Science Foundation of China under Grant Nos. 62101122, 62001103, 61871127, 61701108, 61571117 and 61631007, Natural Science Foundation of Jiangsu Province under Grant BK20210212, the 111 Project under Grant No. 111-2-05, and the Scientific Research Foundation of Graduate School of Southeast University.

H. C. Zhang, L. P. Zhang, S. Liu and Z. Mao contributed equally to this work. We also thank Guangdong Baizi Electronic Tech. Co., Ltd. for helping us build the customized far-field measurement system.

REFERENCES

[1] Rocca, P., G. Oliveri, R. J. Mailloux, and A. Massa, "Unconventional phased array architectures and design methodologies — A review," *Proceedings of the IEEE*, Vol. 104, No. 3, 544–560, 2016.

[2] Nanzer, J. A., S. R. Mghabghab, S. M. Ellison, and A. Schlegel, "Distributed phased arrays: Challenges and recent advances," *IEEE Transactions on Microwave Theory and Techniques*, Vol. 69, No. 11, 4893–4907, 2021.

[3] Brookner, E., "Phased-array and radar breakthroughs," in *2007 IEEE Radar Conference*, 37–42, Waltham, MA, USA, Apr. 2007.

[4] Antonik, P., M. C. Wicks, H. D. Griffiths, and C. J. Baker, "Frequency diverse array radars," in *2006 IEEE Conference on Radar*, 215–217, Verona, NY, USA, Apr. 2006.

[5] Wang, W.-Q., "Adaptive RF stealth beamforming for frequency diverse array radar," in *2015 23rd European Signal Processing Conference (EUSIPCO)*, 1158–1161, Nice, France, Aug. 2015.

[6] Sammartino, P. F. and C. J. Baker, "The frequency diverse bistatic system," in *2009 International Waveform Diversity and Design Conference*, 155–159, Kissimmee, FL, USA, Feb. 2009.

[7] Daly, M. P., E. L. Daly, and J. T. Bernhard, "Demonstration of directional modulation using a phased array," *IEEE Transactions on Antennas and Propagation*, Vol. 58, No. 5, 1545–1550, 2010.

[8] Ding, Y., J. Zhang, and V. Fusco, "Frequency diverse array OFDM transmitter for secure wireless communication," *Electronics Letters*, Vol. 51, No. 17, 1374–1376, 2015.

[9] Eker, T., S. Demir, and A. Hizal, "Exploitation of linear frequency modulated continuous waveform (LFMCW) for frequency diverse arrays," *IEEE Transactions on Antennas and Propagation*, Vol. 61, No. 7, 3546–3553, 2013.

[10] Tan, M., C.-Y. Wang, Z.-H. Li, X. Li, and L. Bao, "Stepped frequency pulse frequency diverse array radar for target localization in angle and range domains," *International Journal of Antennas and Propagation*, Vol. 2018, No. 1, 8962048, 2018.

[11] Wang, W.-Q. and H. Shao, "Range-angle localization of targets by a double-pulse frequency diverse array radar," *IEEE Journal of Selected Topics in Signal Processing*, Vol. 8, No. 1, 106–114, 2014.

[12] Wang, C., J. Xu, G. Liao, X. Xu, and Y. Zhang, "A range ambiguity resolution approach for high-resolution and wide-swath sar imaging using frequency diverse array," *IEEE Journal of Selected Topics in Signal Processing*, Vol. 11, No. 2, 336–346, 2017.

[13] Khan, W. and I. M. Qureshi, "Frequency diverse array radar with time-dependent frequency offset," *IEEE Antennas and Wireless Propagation Letters*, Vol. 13, 758–761, 2014.

[14] Shi, J., "On time-invariant FDA beam-pattern design based on time-dependent frequency offsets," in *2020 IEEE 11th Sensor Array and Multichannel Signal Processing Workshop (SAM)*, 1–4, Hangzhou, China, June 2020.

[15] Yao, A.-M., W. Wu, and D.-G. Fang, "Frequency diverse array antenna using time-modulated optimized frequency offset to obtain time-invariant spatial fine focusing beampattern," *IEEE Transactions on Antennas and Propagation*, Vol. 64, No. 10, 4434–4446, 2016.

[16] Cheng, Q., J. Zhu, T. Xie, J. Luo, and Z. Xu, "Time-invariant angle-range dependent directional modulation based on time-modulated frequency diverse arrays," *IEEE Access*, Vol. 5, 26 279–26 290, 2017.

[17] Yao, A.-M., W. Wu, and D.-G. Fang, "Solutions of time-invariant spatial focusing for multi-targets using time modulated frequency diverse antenna arrays," *IEEE Transactions on Antennas and Propagation*, Vol. 65, No. 2, 552–566, 2017.

[18] Gui, R., W.-Q. Wang, C. Cui, and H. C. So, "Coherent pulsed-FDA radar receiver design with time-variance consideration: SINR and CRB analysis," *IEEE Transactions on Signal Processing*, Vol. 66, No. 1, 200–214, 2018.

[19] Shao, H., X. Li, W.-Q. Wang, J. Xiong, and H. Chen, "Time-invariant transmit beampattern synthesis via weight design for FDA radar," in *2016 IEEE Radar Conference (RadarConf)*, 1–4, Philadelphia, PA, USA, May 2016.

[20] Xu, Y., A. Wang, and J. Xu, "Range-angle transceiver beamforming based on semicircular-FDA scheme," *IEEE Transactions on Aerospace and Electronic Systems*, Vol. 58, No. 2, 834–843, 2022.

[21] Chen, B., X. Chen, Y. Huang, and J. Guan, "Transmit beampattern synthesis for the FDA radar," *IEEE Antennas and Wireless Propagation Letters*, Vol. 17, No. 1, 98–101, 2018.

[22] Wen, C., Y. Huang, J. Peng, J. Wu, G. Zheng, and Y. Zhang, "Slow-time FDA-MIMO technique with application to STAP radar," *IEEE Transactions on Aerospace and Electronic Systems*, Vol. 58, No. 1, 74–95, 2022.

[23] Wang, W.-Q., "Frequency diverse array antenna: New opportunities," *IEEE Antennas and Propagation Magazine*, Vol. 57, No. 2, 145–152, 2015.

[24] Wang, W.-Q., "Range-angle dependent transmit beampattern synthesis for linear frequency diverse arrays," *IEEE Transactions on Antennas and Propagation*, Vol. 61, No. 8, 4073–4081, 2013.

[25] Xu, W., L. Zhang, H. Bi, P. Huang, and W. Tan, "FDA beampattern synthesis with both nonuniform frequency offset and array spacing," *IEEE Antennas and Wireless Propagation Letters*, Vol. 20, No. 12, 2354–2358, 2021.

[26] Tan, M., C. Wang, Z. Li, J. Bai, and L. Bao, "Adaptive beamforming using frequency diverse MIMO radar with nonlinear frequency offset," in *2020 IEEE 11th Sensor Array and Multichannel Signal Processing Workshop (SAM)*, 1–5, Hangzhou, China, Jun. 2020.

[27] Huang, G., Y. Ding, S. Ouyang, and V. Fusco, "Frequency diverse array with random logarithmically increasing frequency offset," *Microwave and Optical Technology Letters*, Vol. 62, No. 7, 2554–2561, 2020.

[28] Geng, L., Y. Li, W. Cheng, L. Dong, and Y. Tan, "Highly focussed beampattern synthesis in FDA-MIMO radar with multi-carrier transmission," *IET Radar, Sonar & Navigation*, Vol. 17, No. 4, 665–682, 2023.

[29] Gao, K., W.-Q. Wang, H. Chen, and J. Cai, "Transmit beamspace design for multi-carrier frequency diverse array sensor," *IEEE Sensors Journal*, Vol. 16, No. 14, 5709–5714, 2016.

[30] Wang, Y., W. Li, G. Huang, and J. Li, "Time-invariant range-angle-dependent beampattern synthesis for FDA radar targets tracking," *IEEE Antennas and Wireless Propagation Letters*, Vol. 16, 2375–2379, 2017.

[31] Stadtler, T., L. Eifler, and J. L. T. Haseborg, "Double probe near field scanner, a new device for measurements in time domain," in *2003 IEEE Symposium on Electromagnetic Compatibility. Symposium Record (Cat. No.03CH37446)*, Vol. 1, 86–90, Boston, MA, USA, Aug. 2003.

[32] Liu, Y. and B. Ravelo, "Fully time-domain scanning of EM near-field radiated by RF circuits," *Progress In Electromagnetics Research B*, Vol. 57, 21–46, 2014.

[33] Brady, S. H., "Frequency diverse array radar: Signal characterization and measurement accuracy," [Online]. Available: https://api.semanticscholar.org/CorpusID:107634913, 2012.

[34] Garcia-Vidal, F. J., A. I. Fernández-Domínguez, L. Martin-Moreno, H. C. Zhang, W. Tang, R. Peng, and T. J. Cui, "Spoof surface plasmon photonics," *Reviews of Modern Physics*, Vol. 94, No. 2, 025004, May 2022.